

Supporting Information

# Design of D-A<sub>1</sub>-A<sub>2</sub> Covalent Triazine Frameworks via Copolymerization for Photocatalytic Hydrogen Evolution

*Liping Guo,<sup>†,§</sup> Yingli Niu,<sup>‡,§</sup> Shumaila Razzaque,<sup>†</sup> Bien Tan,<sup>\*,†</sup> and Shangbin Jin<sup>\*,†</sup>*

<sup>†</sup> Key Laboratory of Material Chemistry for Energy Conversion and Storage, Ministry of Education, School of Chemistry and Chemical Engineering, Huazhong University of Science and Technology, Luoyu Road No. 1037, 430074, Wuhan, China.

Email: [jinsb@hust.edu.cn](mailto:jinsb@hust.edu.cn); [bien.tan@mail.hust.edu.cn](mailto:bien.tan@mail.hust.edu.cn)

<sup>‡</sup> Department of Physics, School of Science, Beijing Jiaotong University, Shangyuancun No. 3, 100044, Beijing, China.

<sup>§</sup>These two authors contributed equally to this work.

## Table of Content

Section	Content	Page
S-A	Characterization Methods	4
S-B	Synthesis and characterization of Monomers	6
S-C	Structural characterization of <i>ter</i> -CTF-0.7 and CTF-BT	7
S-D	Morphology of CTFs	8
S-E	Porosity of CTFs	9
S-F	TGA and XRD of CTFs	10
S-G	The photocatalytic performance of CTFs without Pt loading.	11
S-H	High-resolution TEM images of Pt loaded CTFs.	12
S-I	Structural comparison of <i>ter</i> -CTF-0.7 before and after photocatalytic process	13
S-J	Effect of the photocatalyst amount on HER performance	14
S-K	Bandgaps and LUMO values of CTFs from experiments	15
S-L	Molecular geometry based on DFT calculations	17
S-M	Femtosecond transient absorption (fs-TA) spectra	18
S-N	EPR measurements of CTF-CBZ, <i>ter</i> -CTF-0.7 and CTF-BT	20
S-O	Synthesis and characterization of control samples	21
S-P	Photocatalytic hydrogen production and photoluminescence spectra of control samples.	25
S-Q	The summery of synthesis of CTFs	26
S-R	Elemental analysis results of CTFs	27
S-S	Photocatalytic performance of CTFs in this system	28

S-T	Comparison of photocatalytic performance according to reported literatures	29
S-U	References	31

## S-A Characterization Methods

Monomer structures were checked with  $^1\text{H}$ -NMR and  $^{13}\text{C}$ -NMR (Bruker Avance III 400MHz). High-resolution mass spectra (HRMS) were recorded on the Thermo Scientific Exactive Plus equipped with ESI ionization source. The structures of CTFs were characterized by Fourier-transformed infrared (FT-IR) spectra (Bruker Vertex 70), X-ray photoelectron spectroscopy (XPS) analysis (Thermo Scientific ESCALAB 250xi) and solid-state  $^{13}\text{C}$  NMR experiments (Bruker Avance II 600MHz). The porous properties of CTFs were measured by nitrogen adsorption and desorption at 77 K (Micromeritics ASAP 2010M). The crystalline structure and thermal stability of CTFs were analyzed by powder X-ray diffraction (XRD) patterns (PANalytical B.V. Empyrean) and thermogravimetric analysis (TGA) (PerkinElmer Instruments, Pyris1). The morphology of CTFs were observed by transmission electron microscopy (TEM) (Talos F200X, FEI) and field emission scanning electron microscope (FSEM) (Nova NanoSEM 450). The optical absorption and emission properties of CTFs were recorded with UV-Visible diffuse reflectance spectra (DRS) (Shimadzu UV-3600) at solid state and photoluminescence (PL) spectra (Edinburgh FLS-960) in DMF solution ( $0.5\text{ mg mL}^{-1}$ ). Electrochemical measurements were carried out with electrochemical workstation (Chenhua, CHI760E). The samples were prepared by mixing ground polymer (2 mg) with ethanol (5 mL) containing 1 wt% Nafion, and then were sonicated 10 min. 100  $\mu\text{L}$  sample was taken and deposited on ITO with the area  $1\text{ cm}^2$ . The transient photocurrent was conducted under visible light irradiation with the fixed time interval. 0.1 M  $\text{Na}_2\text{SO}_4$  solution was selected as supporting electrolyte and the pH value is 7. Electron paramagnetic resonance (EPR) of CTFs were tested (Bruker, JES X320) with the frequency 9.588 GHz and power 10 mW.

The radical of CTFs under visible light irradiation were detected with 5,5-Dimethyl-1-pyrroline N-oxide (DMPO) as the capture agent. At room temperature, the radical of CTFs under visible light irradiation with different time (0 min, 5 min and 10 min) were detected with 5,5-Dimethyl-1-pyrroline N-oxide (DMPO) as the capture agent. 2 mg CTFs was adopted in 1 ml solvent containing 100 mM DMPO. With the presence of oxygen, the superoxide radical of CTFs were examined in menthol solution and the hydroxyl radical of CTFs were examined in water.

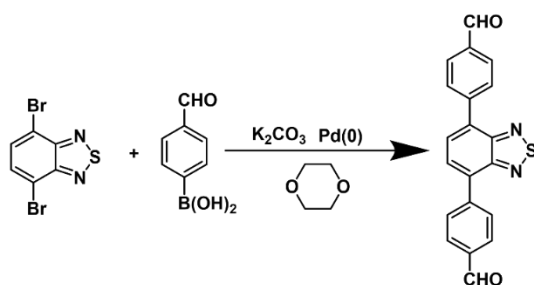
The femtosecond - transient absorption (fs-TA) measurements were performed on a Helios pump-probe system (Ultrafast Systems LLC) combined with an amplified femtosecond laser system (Coherent). The films of samples supported by quartz sheet were obtained with the evaporation of ethanol. 400 nm pump pulse were used in this test provided by a Ti: sapphire regenerative amplifier and the probe pulses were 420-760 nm produced by the 800 nm beams focusing onto a sapphire plate. The temporal and spectral profiles (chirp-corrected) of the pump-induced differential transmission of the white-light continuum (WLC) probe light (i.e., absorbance change) were visualized by an optical fiber-coupled multichannel spectrometer (with a CMOS sensor) and further processed by the Surface Xplorer software.

Density functional theory (DFT) and linear response time-dependent density functional theory (LR-TDDFT) with B3LYP functional and 6-311G (d,p) basis set in Gaussian 16 package were applied to optimize the ground state geometry and to calculate the molecular orbitals and charge density difference between the first excited state and ground state.

## S-B Synthesis and Characterization of Monomers

Monomer-CBZ and terephthalamidine dihydrochloride were synthesized according to the literatures.<sup>1-2</sup>

### Synthesis of Monomer-BT



The mixture of 4,7-dibromo-2,1,3-benzothiadiazole (0.59 g, 2.0 mmol), *p*-tolyl boronic acid (1.18 g, 8.0 mmol) and terakis(triphenylphosphine) palladium (0.12 g, 1.0 mmol) were added in dioxane (16.0 mL), and then the additional aqueous solution of potassium carbonate (27 wt%, 3.6 mL) was added. Under the protection of nitrogen, the suspension was reacted with stirring at 105 °C for 48 h. After that, the crude product was extracted with dichloromethane. The purification of product was conducted by recrystallization from methanol/dichloromethane, and the final product 4,7-bis(4-formylphenyl)-2,1,3-benzothiadiazole was dried under vacuum (0.51 g, 74%). <sup>1</sup>H-NMR (400 MHz, CDCl<sub>3</sub>: ppm): δ = 10.14 (s, 2H, -CHO); δ = 8.18 (d, *J* = 8.0 Hz, 4H, Ar-H); δ = 8.08 (d, *J* = 8.0 Hz, 4H, Ar-H); δ = 7.92 (s, 2H, Ar-H). <sup>13</sup>C-NMR (75 MHz, CDCl<sub>3</sub>: ppm): 191.83; 153.76; 142.93; 136.04; 132.99; 130.00; 128.69. HR-MS: *m/z* (%): 345.0675 (100, [*M*+H]<sup>+</sup>, calcd for C<sub>20</sub>H<sub>13</sub>N<sub>2</sub>O<sub>2</sub>S<sup>+</sup>: 345.06)

## S-C Structural Characterization of *ter*-CTF-0.7 and CTF-BT

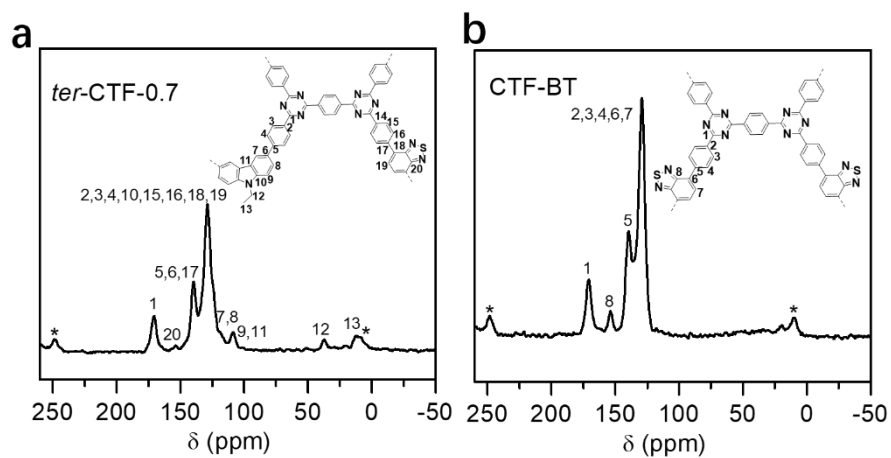


**Figure S1.** The solid-state  $^{13}\text{C}$ -NMR spectra of *ter*-CTF-0.7 (a) and CTF-BT (b).

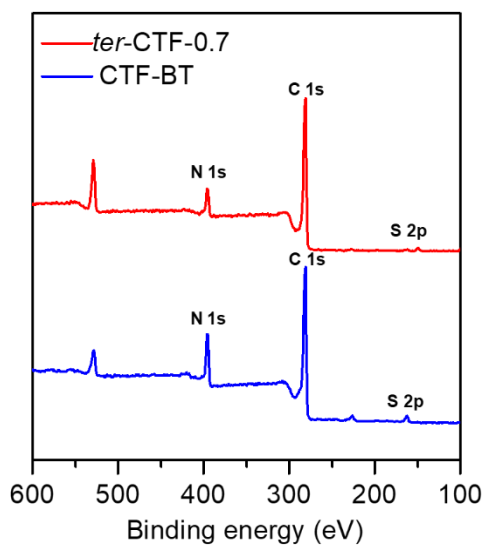


**Figure S2.** The XPS survey of *ter*-CTF-0.7 and CTF-BT.

## S-D Morphology of CTFs

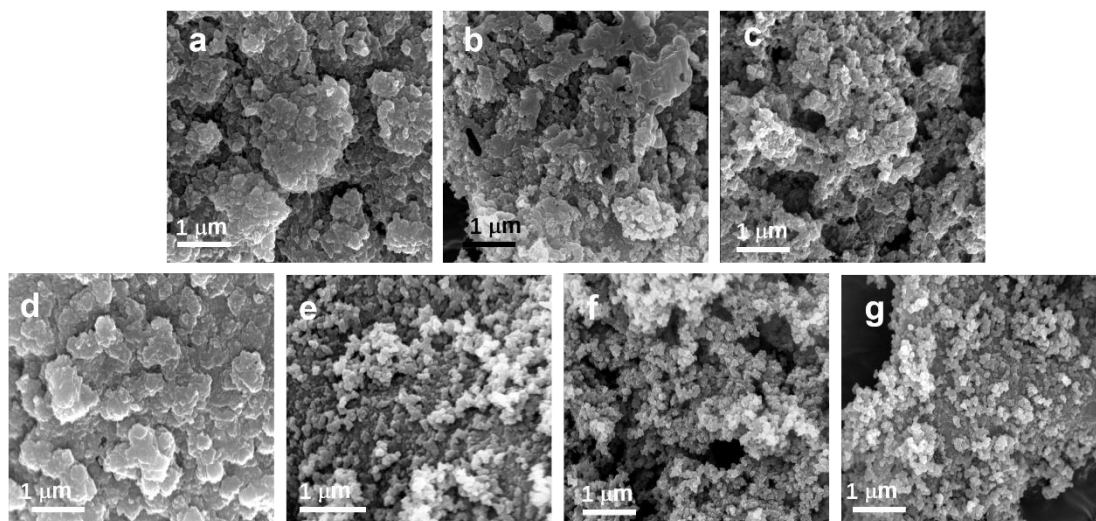


**Figure S3.** SEM images of CTFs: (a) CTF-CBZ; (b) *ter*-CTF-0.9; (c) *ter*-CTF-0.8; (d) *ter*-CTF-0.7; (e) *ter*-CTF-0.6; (f) *ter*-CTF-0.5; (g) CTF-BT.

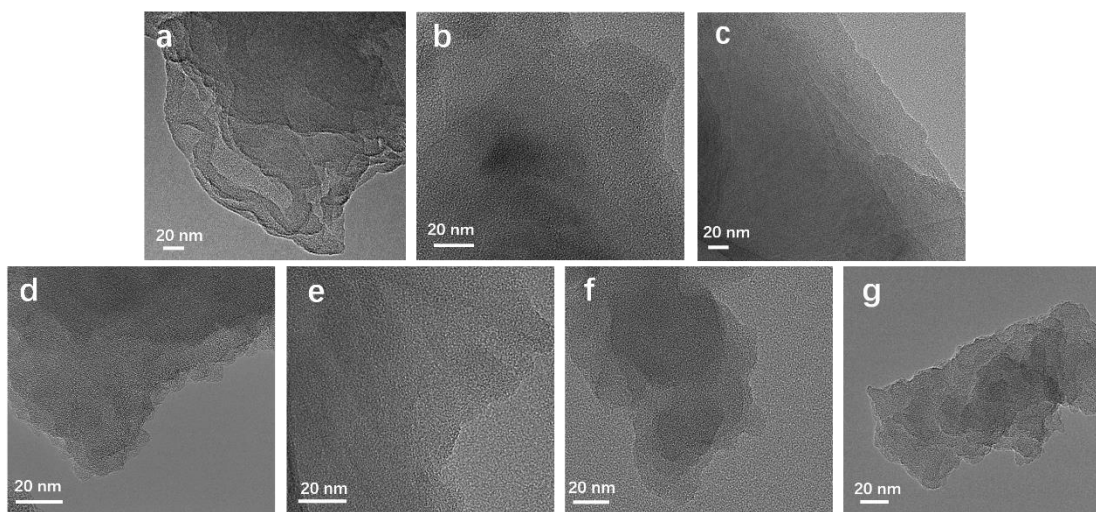


**Figure S4.** TEM images of CTFs: (a) CTF-CBZ; (b) *ter*-CTF-0.9; (c) *ter*-CTF-0.8; (d) *ter*-CTF-0.7; (e) *ter*-CTF-0.6; (f) *ter*-CTF-0.5; (g) CTF-BT.



## S-E Porosity of CTFs

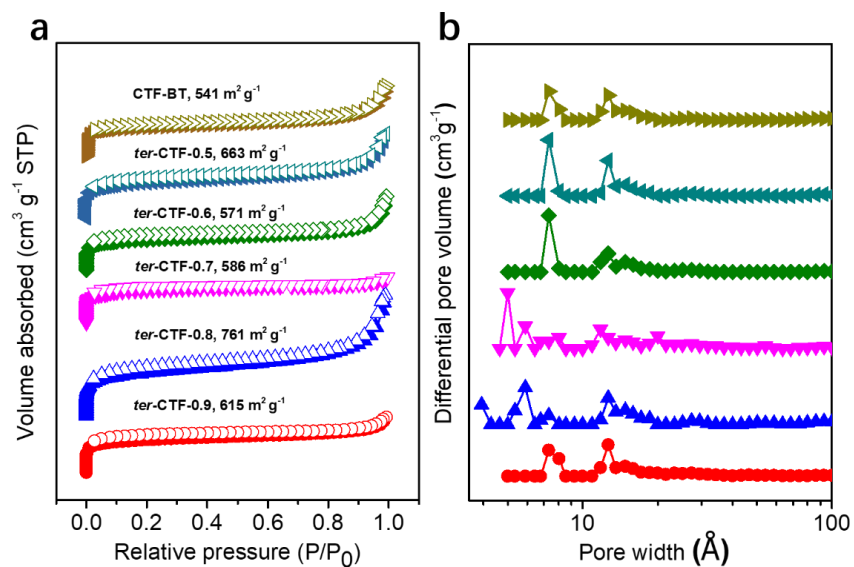


**Figure S5.** Nitrogen sorption curves (a) and corresponding pore size distributions (b) of CTFs.

## S-F TGA and PXRD of CTFs

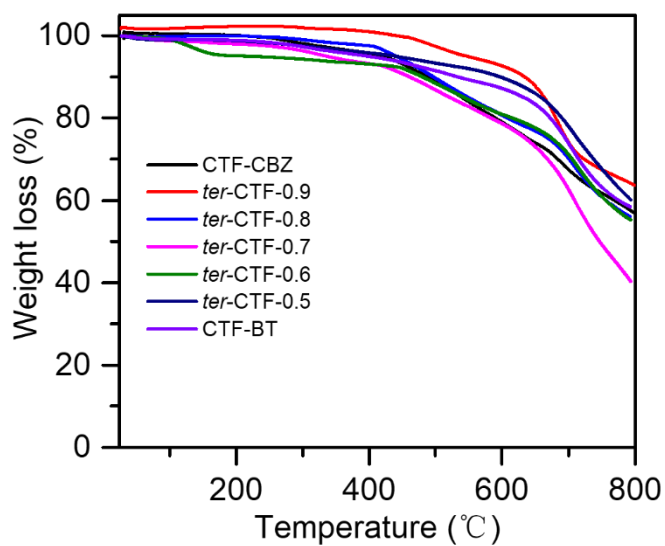


**Figure S6.** TG curves of CTFs under N<sub>2</sub> atmosphere.

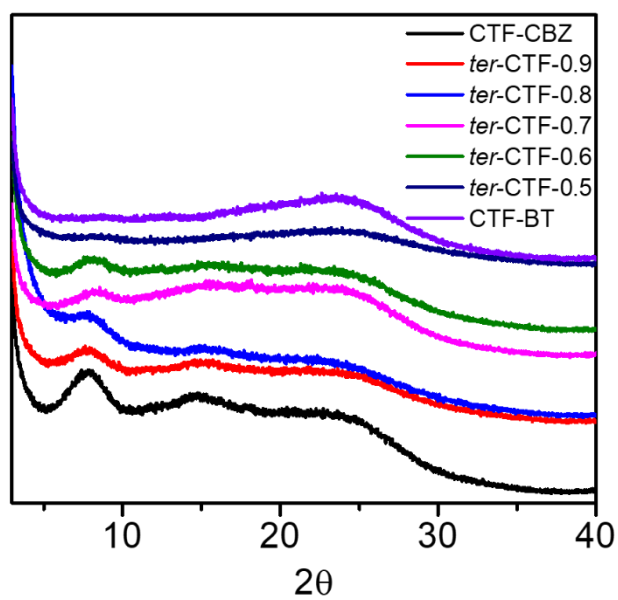


**Figure S7.** Powder X-ray diffraction patterns of CTFs.

**S-G The photocatalytic performance of CTFs without Pt loading.**

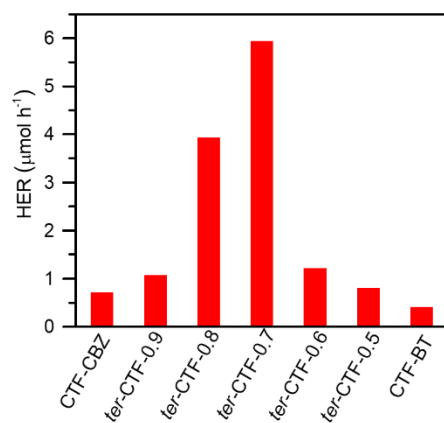


**Figure S8.** The HER of CTFs without Pt loading.

## S-H High-Resolution TEM images of Pt Loaded CTFs.

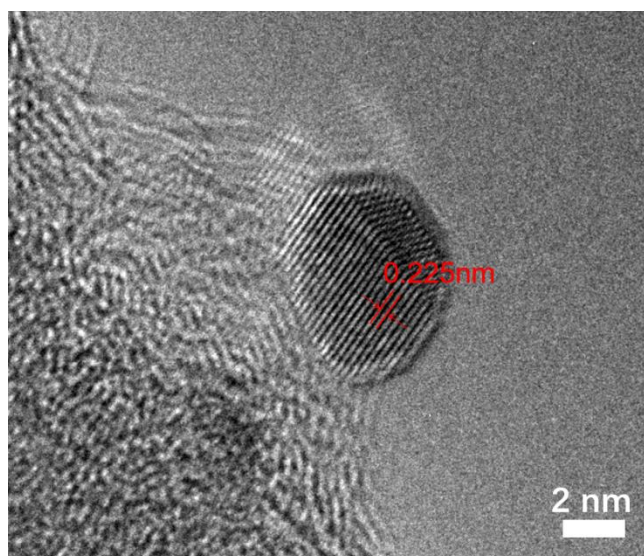


**Figure S9.** The Pt morphology on the surface of *ter*-CTF-0.7.

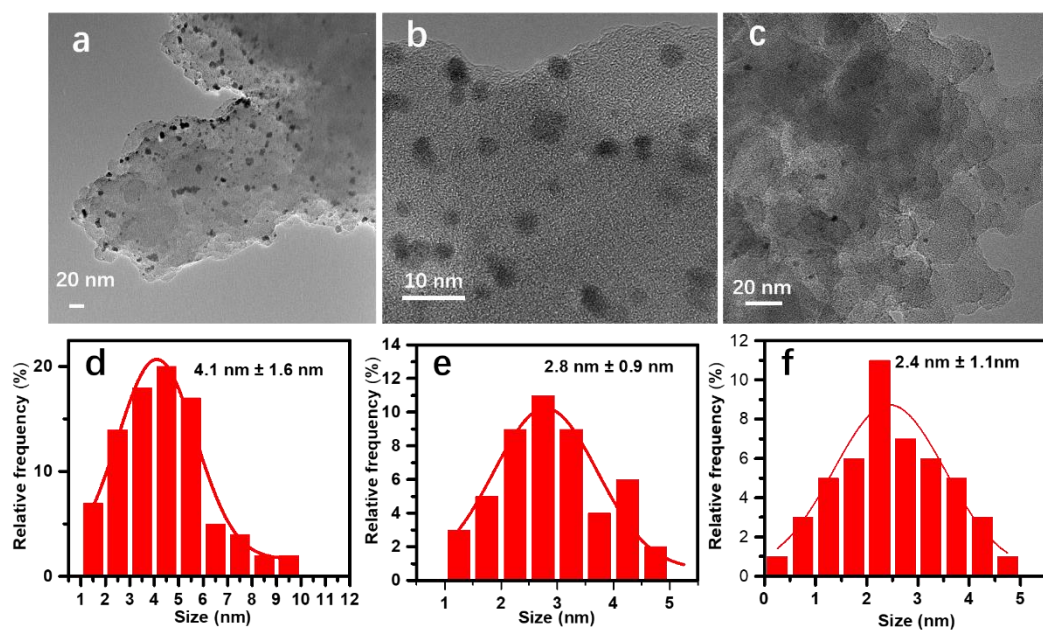


**Figure S10.** High-resolution TEM image after loading Pt nanoparticles and Pt distribution of CTF-CBZ (a, d), *ter*-CTF-0.7 (b, e) and CTF-BT (c, f).

## S-I Structural Comparison of *ter*-CTF-0.7 Before and After Photocatalytic Process

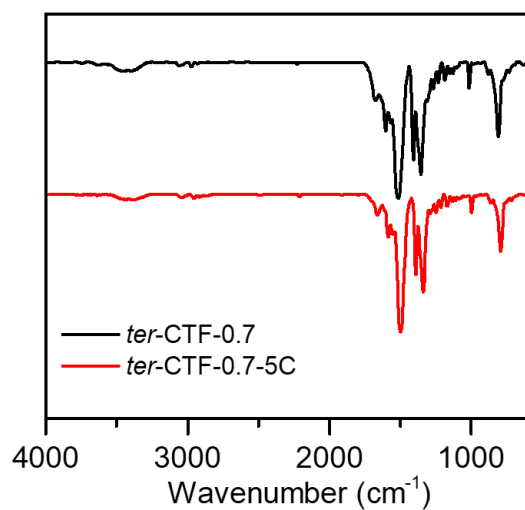


**Figure S11.** FT-IR spectra of corresponding *ter*-CTF-0.7 before and after 5 cycles photocatalytic process.

### S-J Effect of the Photocatalyst Amount on HER Performance

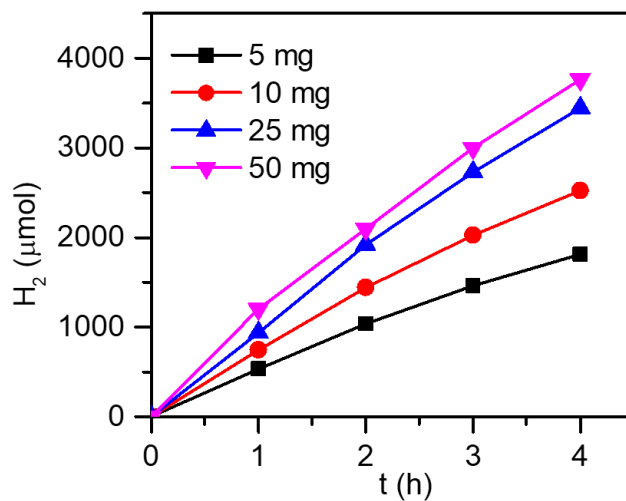


**Figure S12.** Time course of H<sub>2</sub> production of *ter*-CTF-0.7 with different contents.

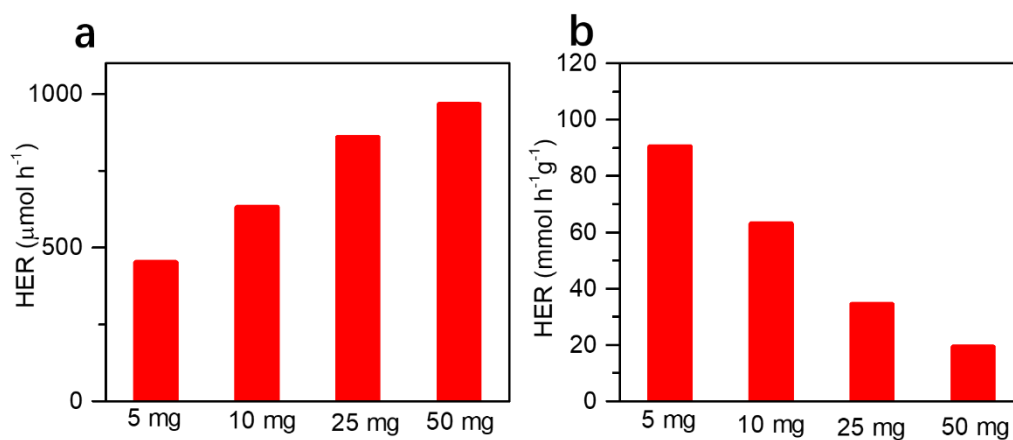


**Figure S13.** HER of H<sub>2</sub> production of *ter*-CTF-0.7 with different contents with different unit (a) μmol h<sup>-1</sup> and (b) mmol h<sup>-1</sup>g<sup>-1</sup>.

## S-K Bandgaps and LUMO values of CTFs from Experiments

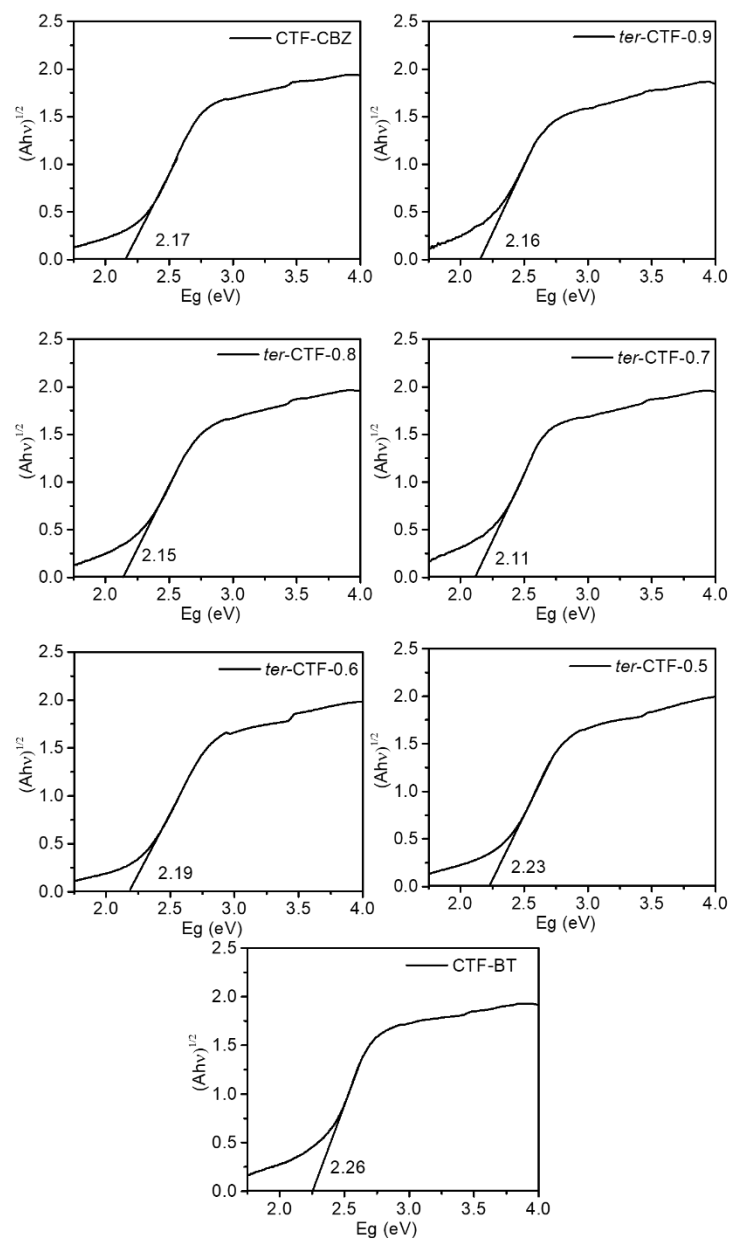


**Figure S14.** The bandgaps of CTFs calculated by Tauc-plot.

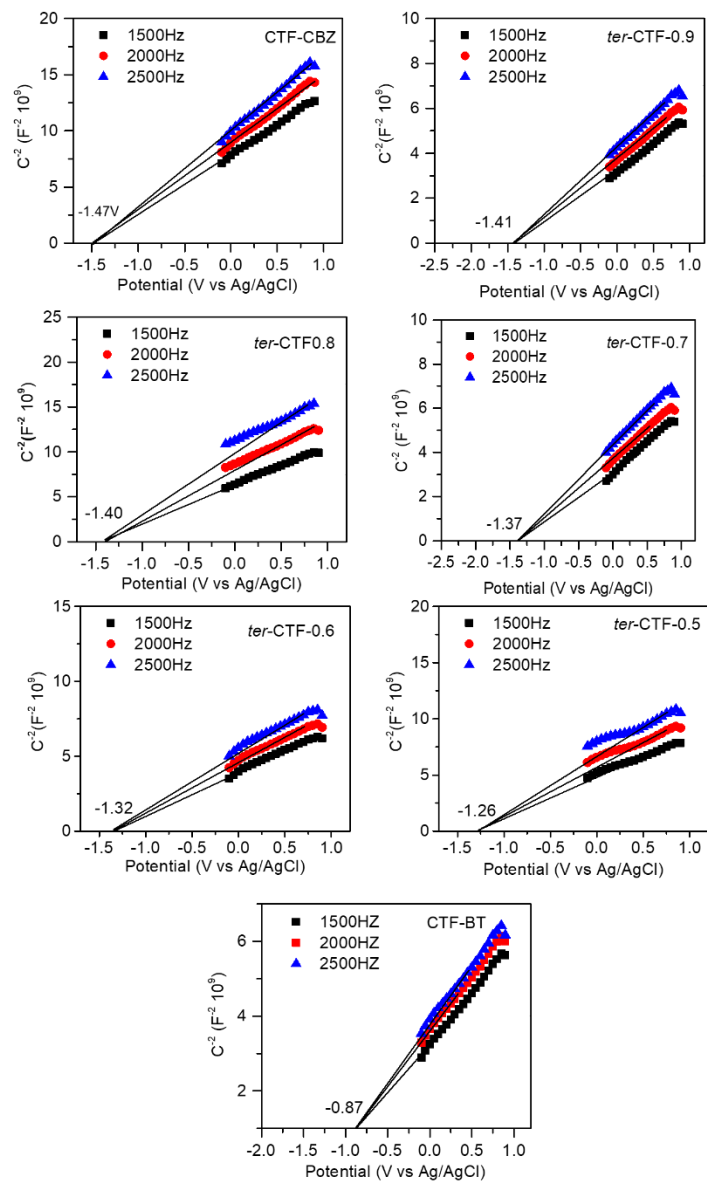


**Figure S15.** Mott-Schottky plots of CTFs.



## S-L Molecular Geometry based on DFT Calculations

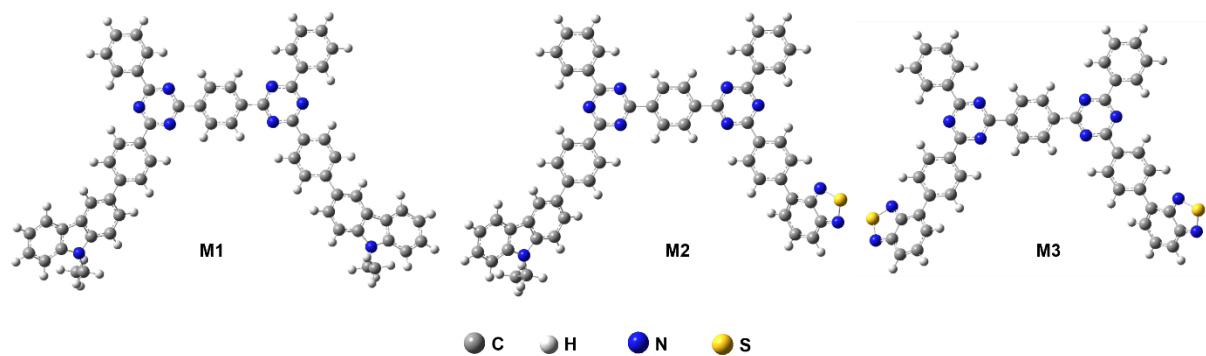


**Figure S16.** Molecular geometry based on DFT calculations.

## S-M Femtosecond transient absorption (fs-TA) spectra

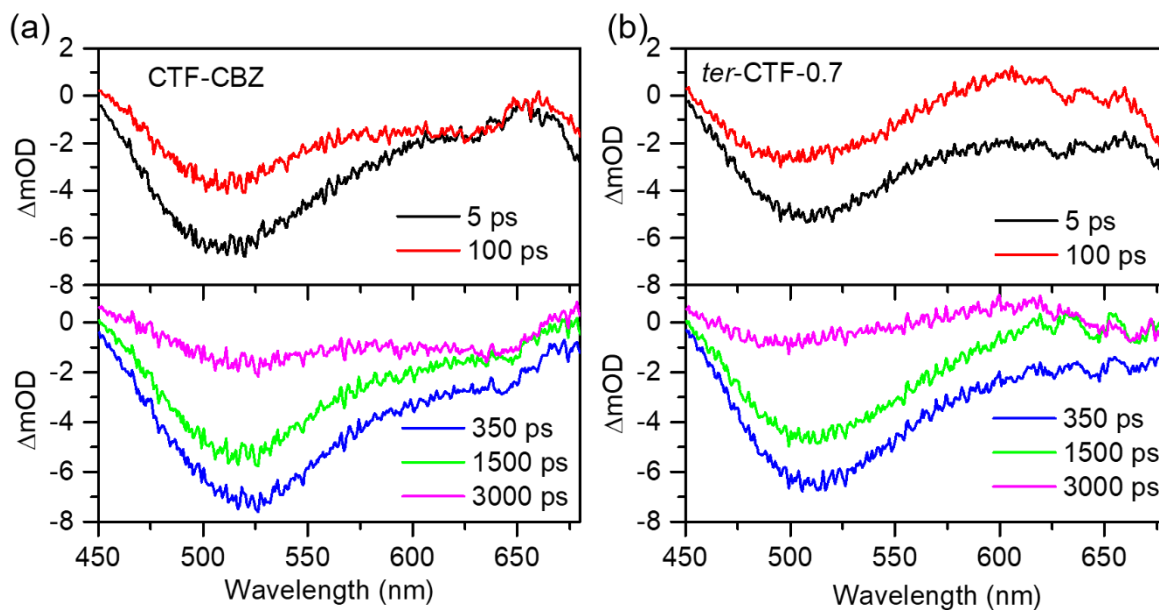


**Figure S17.** Femtosecond transient absorption spectra of CTF-CBZ (a) and *ter*-CTF-0.7 (b).

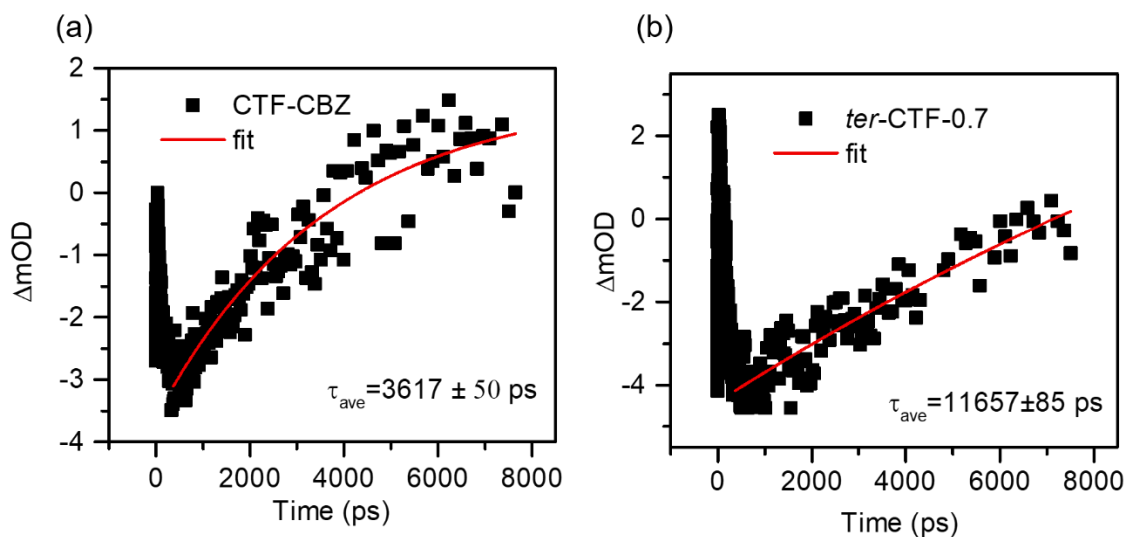


**Figure S18.** The overall decay kinetics of CTF-CBZ (a) and *ter*-CTF-0.7 (b) at 521 nm.

### S-N EPR Measurements of CTF-CBZ, *ter*-CTF-0.7 and CTF-BT

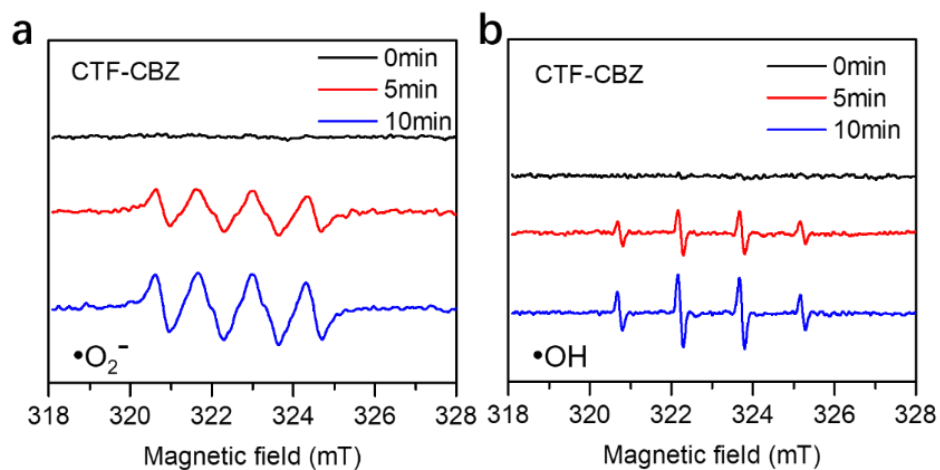


**Figure S19.** EPR spectrum of CTF-CBZ sample: a) superoxide radical and b) hydroxyl radical.

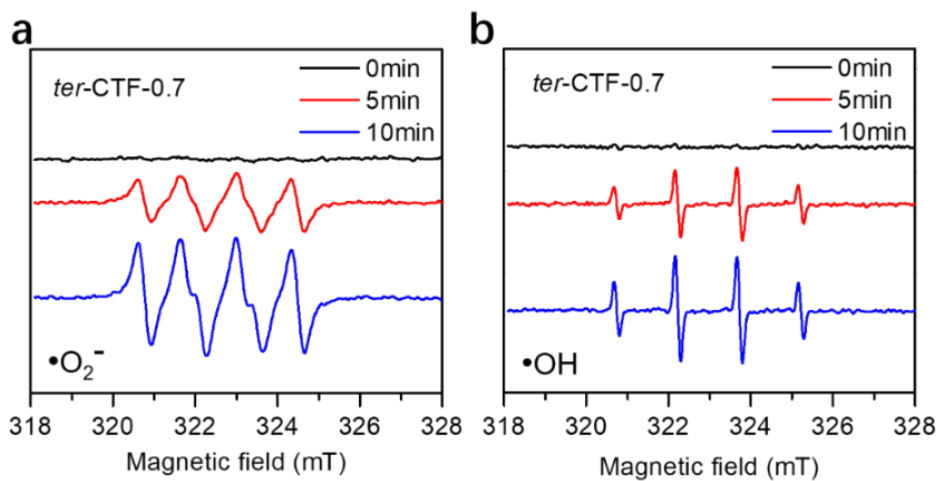


**Figure S20.** EPR spectrum of *ter*-CTF-0.7 sample: a) superoxide radical and b) hydroxyl radical.

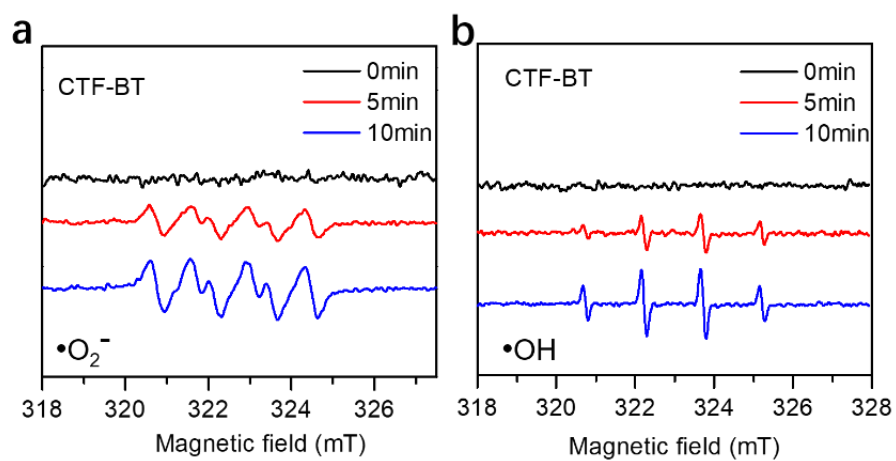
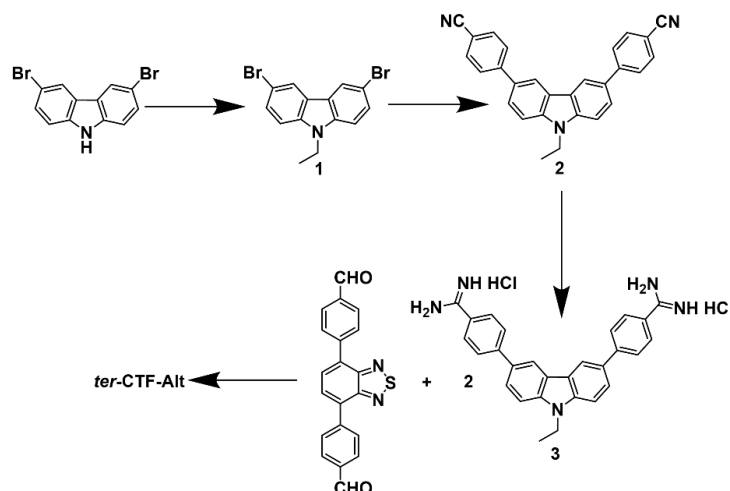


**Figure S21.** EPR spectrum of CTF-BT sample: a) superoxide radical and b) hydroxyl radical.

## S-O Synthesis and Characterizations of Control Samples



**Scheme S1.** Synthesis route of *ter*-CTF-Alt.

### Synthesis of 3,6-dibenzonitrile-9-ethylcarbazole (Compound 2):

Compound 1 was synthesized according to the reported method.<sup>3</sup> The mixture of 3,6-dibromo-9-ethylcarbazole (1.4 g, 4 mmol) and 4-cyanophenylboronic acid (1.8 g, 12 mmol) and terakis(triphenylphosphine) palladium (0.24 g, 2.0 mmol) was added in dioxane (30.0 mL), and then the additional aqueous solution of potassium carbonate (27 wt%, 7 mL) was added. Under the protection of nitrogen, the suspension was reacted with stirring at 105 °C for 36 h. After that, the crude product was extracted with dichloromethane. The purification of product was conducted by recrystallization from methanol/dichloromethane, and the final product 4,4'-(9-ethyl-9H-carbazole-3,6-diyl)dibenzonitrile was achieved after dried under vacuum (1.1 g, 69%). <sup>1</sup>H-NMR (400MHz, CDCl<sub>3</sub>): δ = 8.39 (s, 2H, Ar-H); δ = 7.83 (d, *J* = 8.0 Hz, 4H, Ar-H); δ = 7.76 (d, *J* = 8.0 Hz, 6H, Ar-H); δ = 7.54 (d, *J* = 8.0 Hz, 2H, Ar-H); δ = 4.46 (q, *J* = 7.2 Hz, 2H, -CH<sub>2</sub>-); δ = 1.51 (t, 3H, -CH<sub>3</sub>). <sup>13</sup>C-NMR (75 MHz, CDCl<sub>3</sub>: ppm): 146.36; 140.64; 132.66; 130.61; 127.66; 125.59; 123.61; 119.38; 119.23; 109.71; 109.45; 38.02; 13.94. HR-MS: *m/z* (%): 398.1646 (100, [M+H]<sup>+</sup>, calcd for C<sub>28</sub>H<sub>20</sub>N<sub>3</sub><sup>+</sup>: 398.16).

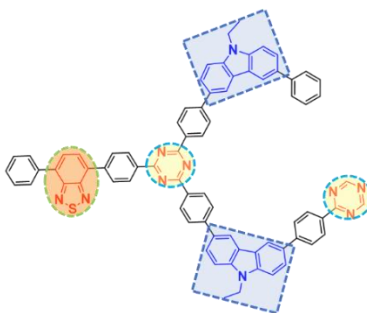
### Synthesis of 3,6-dibenzimidamide-9-ethylcarbazole dihydrochloride (Compound 3):

3,6-dibromo-9-ethylcarbazole (0.6 g, 1.5 mmol) was added into 10 mL THF solution, and then lithium bis(trimethylsilyl)amide (0.01 mmol, 10 mL) was added dropwise at ice-water bath. After that, the mixture was heated at 25 °C with stirring about 6 h. then the ethanol 10 mL solution containing 45% (v/v) acetyl chloride was added drop by drop at ice-water bath. The precipitate was wash with ether and water. The yellow product was obtained through recrystallization with THF (0.41 g, 54%). <sup>1</sup>H-NMR (400MHz, DMSO: ppm): δ = 9.48 (s, 4H, -NH<sub>2</sub>); δ = 9.22 (s, 4H, =NH<sub>2</sub><sup>+</sup>); δ = 8.86 (s, 2H, Ar-H); δ = 8.11 (d, *J* = 8.00 Hz, 4H, Ar-H); δ = 8.01 (d, *J* = 8.00 Hz, 4H, Ar-H); δ = 7.98 (d, *J* = 8 Hz, 2H, Ar-H); δ = 7.80 (d, *J* = 8 Hz, 2H, Ar-H); δ = 4.56 (q, *J* = 6.8 Hz, 2H, -CH<sub>2</sub>-); δ = 1.38 (t, 3H, -CH<sub>3</sub>). <sup>13</sup>C-NMR (75 MHz, DMSO: ppm): 165.64; 146.55; 140.86; 129.78; 129.27; 127.09; 125.96; 125.77; 123.66; 120.00; 110.59; 37.83; 14.16. HR-MS: *m/z* (%): 432.2227 (100, [*M*+H]<sup>+</sup>, calcd for C<sub>18</sub>H<sub>26</sub>N<sub>2</sub><sup>+</sup>: 432.54)

### Synthesis of *ter*-CTF-Alt

The mixture of 4,7-bis(4-formylphenyl)-2,1,3-benzothiadiazole (0.17 g, 0.5 mmol) and 3,6-dibenzimidamide-9-ethylcarbazole dihydrochloride (0.50 g, 1.0 mmol) and Cs<sub>2</sub>CO<sub>3</sub> (0.65 g, 2.0 mmol) were dissolved into 20.0 mL DMSO, and heated at 60 °C, 80 °C, 100 °C, 120 °C and 150 °C, through temperature-programmed route with stirring. Then the suspension is cooled to room temperature, and the polymer was collected by filtration, washed with water, DMF and then freeze-drying. The final product *ter*-CTF-Alt was obtained as an orange-red powder (0.44 mg, 77%).

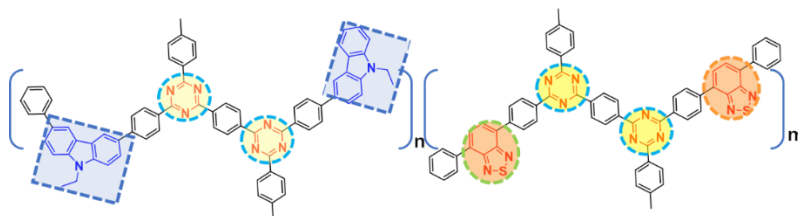
The possible model fragments of the *ter*-CTF-Alt is shown as following:



### Synthesis of *ter*-CTF-0.7-Blo:

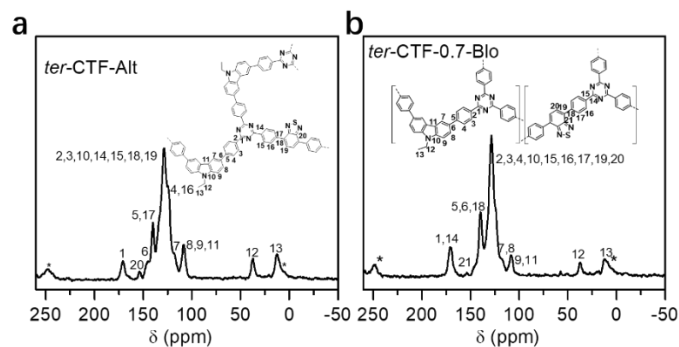
The mixture of 3,6-dicarbaldehyde-N-ethylcarbazole (M-CBZ, 0.27 g, 0.7 mmol), terephthalamidine dihydrochloride (0.47 g, 2.0 mmol) and  $\text{Cs}_2\text{CO}_3$  (1.31 g, 4.0 mmol) were dissolved into 40.0 mL DMSO, and heated through temperature-programmed route with stirring at 60 °C for 12 h. After that, 4,7-bis(4-formylphenyl)-2,1,3-benzothiadiazole (M-BT, 0.10 g, 0.3 mmol) was added and then heated to 80 °C for 12 h, 100 °C for 12 h, 120 °C for 36 h and 150 °C for 36 h. Finally, the suspension cooled to room temperature, and the polymer was washed with water and DMF, then freeze-dried. The resulting product *ter*-CTF-0.7-Blo was obtained as a yellow powder (yield: 74%).

The possible model structure of *ter*-CTF-0.7-Blo is describe as following:

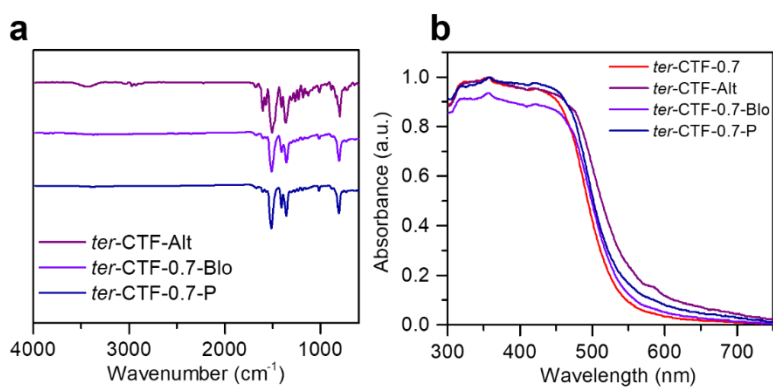


### Synthesis of *ter*-CTF-0.7-P:

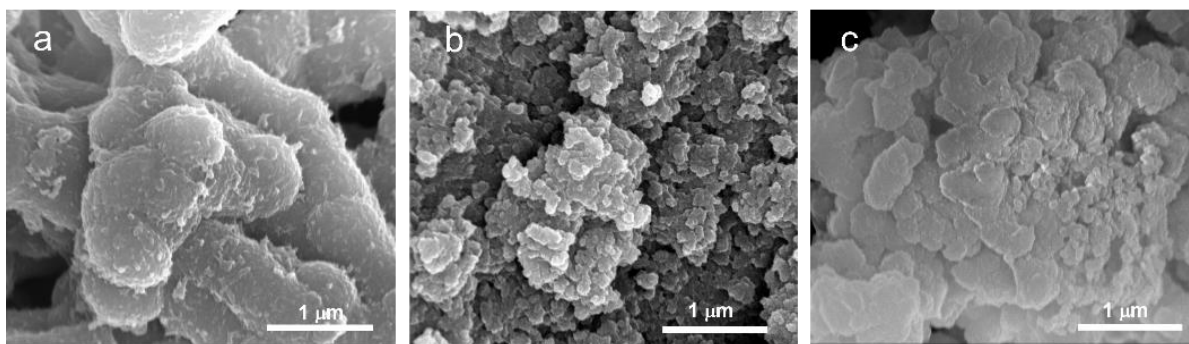
CTF-CBZ and CTF-BT were physically mixed with each other at the mass ratio of 0.7:0.3 in ethanol solution. After stirring 4 hours, the final polymer was obtained with rotary evaporated and was abbreviated as *ter*-CTF-0.7-P.



**Figure S22.** The solid-state  $^{13}\text{C}$ -NMR spectra of *ter*-CTF-Alt (a) and *ter*-CTF-0.7-Blo (b).



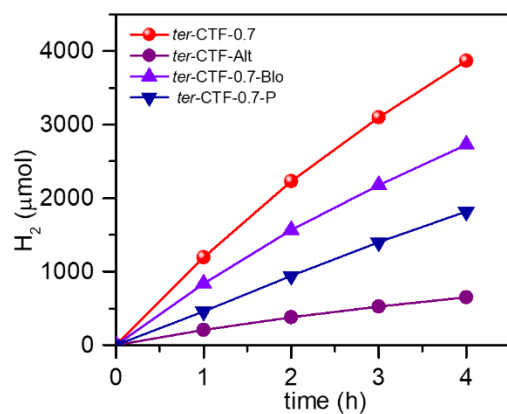
**Figure S23.** FT-IR (a) and DRS spectra (b) of control samples.



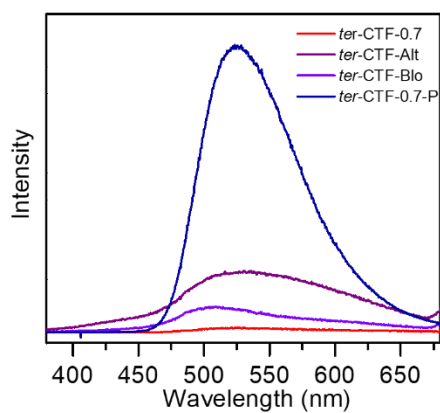
**Figure S24.** SEM images of control samples: (a) *ter*-CTF-Alt; (b) *ter*-CTF-0.7-Blo; (c) *ter*-CTF-0.7-P.



## S-P Photocatalytic Hydrogen Production and Photoluminescence Spectra of Control Samples.



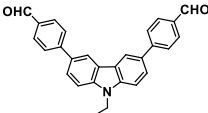
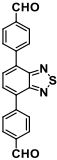
**Figure S25.** Photocatalytic performance of the control samples.



**Figure S26.** Photoluminescence spectra of the control samples.

## S-Q Summary of Synthesis of CTFs

**Table S1** The summary of synthesis of CTFs.

Entry			Yield (%)	BET (m <sup>2</sup> /g)	Bandgap (eV)
<b>CTF-CBZ</b>	1	0	62	650	2.17
<b><i>ter</i>-CTF-0.9</b>	0.9	0.1	75	615	2.16
<b><i>ter</i>-CTF-0.8</b>	0.8	0.2	83	761	2.15
<b><i>ter</i>-CTF-0.7</b>	0.7	0.3	85	586	2.11
<b><i>ter</i>-CTF-0.6</b>	0.6	0.4	87	571	2.19
<b><i>ter</i>-CTF-0.5</b>	0.5	0.5	87	663	2.23
<b>CTF-BT</b>	0	1	90	541	2.26

## S-R Elemental Analysis Results of CTFs

**Table S2** Elemental analysis results of CTFs.

<b>Sample</b>	<b>N (%)<sup>a</sup></b>	<b>N (%)<sup>b</sup></b>	<b>C (%)<sup>a</sup></b>	<b>C (%)<sup>b</sup></b>	<b>H (%)<sup>a</sup></b>	<b>H (%)<sup>b</sup></b>	<b>S (%)<sup>a</sup></b>	<b>S (%)<sup>b</sup></b>
<b>CTF-BT</b>	17.37	20.50	65.91	70.32	3.52	3.32	4.57	5.87
<b><i>ter</i>-CTF-0.5</b>	16.10	17.50	70.65	76.05	3.85	3.78	2.85	2.67
<b><i>ter</i>-CTF-0.6</b>	15.04	16.96	71.67	77.05	4.12	3.89	1.99	2.10
<b><i>ter</i>-CTF-0.7</b>	15.19	16.45	72.03	78.06	3.97	3.94	1.90	1.55
<b><i>ter</i>-CTF-0.8</b>	15.28	15.95	74.07	79.02	4.04	4.02	1.17	1.01
<b><i>ter</i>-CTF-0.9</b>	14.45	16.00	74.44	79.25	4.62	4.23	0.92	0.52
<b>CTF-CBZ<sup>1</sup></b>	14.00	15.10	74.90	81.3	4.50	3.60	/	/

<sup>a</sup>)The average elemental content of twice measurements;

<sup>b</sup>)Theoretical elemental content calculated based on infinite network structures.

## S-S Photocatalytic Performance of CTFs in this system

Table S3 Photocatalytic performance of CTFs.

CTFs	HER ( $\mu\text{mol h}^{-1}$ , 50 mg)	AQY-420 nm (%)	AQY-500 nm (%)	Pt (%)
<b>CTF-CBZ<sup>1</sup></b>	496	4.07	2.79	2.11
<b><i>ter</i>-CTF-0.9</b>	580	9.49	8.45	1.98
<b><i>ter</i>-CTF-0.8</b>	878	20.00	15.51	2.07
<b><i>ter</i>-CTF-0.7</b>	966	22.86	14.78	1.95
<b><i>ter</i>-CTF-0.6</b>	766	15.36	12.48	2.13
<b><i>ter</i>-CTF-0.5</b>	490	6.8	3.16	1.91
<b>CTF-BT</b>	182	1.67	1.39	1.99

## S-T Comparison of Photocatalytic Performance to Reported Literatures

**Table S4** Photocatalytic performance of the reported organic and inorganic materials.

Photocatalyst	Photocatalytic Conditions	HER ( $\mu\text{mol h}^{-1}$ )	AQY	Ref
<b>CTF-1-100w</b>	>420 nm, TEOA and MeOH, 3 wt% Pt, 50 mg	275	6.0% (420 nm)	4
<b>CTF-1-10 min</b>	>420 nm, TEOA, Pt, 25 mg	26.8	9.2% (420 nm)	5
<b>FS-COF-WS5F</b>	>420 nm, ascorbic acid, 0.038 wt% Pt, 5 mg	81.5	2.2% (600 nm)	6
<b>N3-COF</b>	>420 nm, TEOA, 3wt%Pt, 5 mg	9	0.45%(450 nm)	7
<b>CMP-PyDOBT-1</b>	>420 nm, TEOA, 3 wt% Pt, 50 mg	426	6.1% (400 nm)	8
<b>PCP-10</b>	>420 nm, TEA, 2 wt%, 12 mg	31.7	1.93% (400 nm)	9
<b>Conjugated polybenzodiazoles</b>	>420 nm, TEOA, 3 wt% Pt, 50 mg	116	4.0% (420 nm)	10
<b>P3/CN</b>	>420 nm, TEOA, Pt, 50 mg	650	14.97%(420 nm)	11

<b>NH<sub>2</sub>-UiO-66/ TpPa-1-COF</b>	> 420nm, 0.2% sodium ascorbate; 3 wt% Pt, 10 mg	234.1	/	12
<b>Ni<sub>2</sub>P/MIL-125- NH<sub>2</sub></b>	>420 nm, TEA, 17 mg	15.2	27% (400 nm) 6.6% (450 nm)	13
<b>ter-CTF-0.7</b>	>420 nm, TEOA, ~2 wt% Pt 50 mg	<b>966</b>	<b>22.8% (420 nm)</b> <b>14.7% (500 nm)</b>	<b><i>This work</i></b>

## S-U References

- [1] Guo, L.; Niu, Y.; Xu, H.; Li, Q.; Razzaque, S.; Huang, Q.; Jin, S.; Tan, B. Engineering Heteroatoms with Atomic Precision in Donor–Acceptor Covalent Triazine Frameworks to Boost Photocatalytic Hydrogen Production. *J. Mater. Chem. A*. **2018**, *6*, 19775-19781.
- [2] Wang, K.; Yang, L.; Wang, X.; Guo, L.; Cheng, G.; Zhang, C.; Jin, S.; Tan, B.; Cooper, A. Covalent Triazine Frameworks via a Low Temperature Polycondensation Approach. *Angew. Chem. Int. Ed.* **2017**, *56*, 14149.
- [3] Shen, J. Y.; Yang, X. L.; Huang, T. H.; Lin, J. T.; Ke, T. H.; Chen, L. Y.; Wu, C. C.; Yeh, M. C. P. Ambipolar Conductive 2,7-Carbazole Derivatives For Electroluminescent Devices. *Adv. Funct. Mater.* **2007**, *17*, 983-995.
- [4] Xie, J.; Shevlin, S. A.; Ruan, Q.; Moniz, S. J. A.; Liu, Y.; Liu, X.; Li, Y.; Lau, C. C.; Guo, Z. X.; Tang, J. Efficient Visible Light-Driven Water Oxidation and Proton Reduction by an Ordered Covalent Triazine-Based Framework. *Energ. Environ. Sci.* **2018**, *11*, 1617-1624.
- [5] Kuecken, S.; Acharjya, A.; Zhi, L.; Schwarze, M.; Schomaecker, R.; Thomas, A. Fast Tuning of Covalent Triazine Frameworks for Photocatalytic Hydrogen Evolution. *Chem. Commun.* **2017**, *53*, 5854-5857.
- [6] Wang, X.; Chen, L.; Chong, S. Y.; Little, M. A.; Wu, Y.; Zhu, W. H.; Clowes, R.; Yan, Y.; Zwijnenburg, M. A.; Sprick, R. S.; Cooper, A. I. Sulfone-Containing Covalent Organic Frameworks for Photocatalytic Hydrogen Evolution from Water. *Nat. Chem.* **2018**, *10*, 1180-1189.
- [7] Vyas, V. S.; Haase, F.; Stegbauer, L.; Savasci, G.; Podjaski, F.; Ochsenfeld, C.; Lotsch, B. V. A Tunable Azine Covalent Organic Framework Platform for Visible Light-Induced Hydrogen Generation. *Nat. Commun.* **2015**, *6*, 8508.
- [8] Zhao, Y.; Ma, W.; Xu, Y.; Zhang, C.; Wang, Q.; Yang, T.; Gao, X.; Wang, F.; Yan, C.; Jiang, J.X. Effect of Linking Pattern of Dibenzothiophene-S,S-dioxideContaining Conjugated Microporous Polymers on the Photocatalytic Performance. *Macromolecules*. **2018**, *51*, 9502-9508.
- [9] Li, L.; Lo, W.-y.; Cai, Z.; Zhang, N.; Yu, L. Donor–Acceptor Porous Conjugated Polymers for Photocatalytic Hydrogen Production: The Importance of Acceptor Comonomer. *Macromolecules*. **2016**, *49*, 6903-6909.

- [10] Yang, C.; Ma, B. C.; Zhang, L.; Lin, S.; Ghasimi, S.; Landfester, K.; Zhang, K. A.; Wang, X. Molecular Engineering of Conjugated Polybenzothiadiazoles for Enhanced Hydrogen Production by Photosynthesis. *Angew. Chem. Int. Ed.* **2016**, *55*, 9202-9206.
- [11] Yu, F.; Wang, Z.; Zhang, S.; Ye, H.; Kong, K.; Gong, X.; Hua, J.; Tian, H. Molecular Engineering of Donor-Acceptor Conjugated Polymer/g-C<sub>3</sub>N<sub>4</sub> Heterostructures for Significantly Enhanced Hydrogen Evolution Under Visible-Light Irradiation. *Adv. Funct. Mater.* **2018**, 1804512.
- [12] Zhang, F. M.; Sheng, J. L.; Yang, Z. D.; Sun, X. J.; Tang, H. L.; Lu, M.; Dong, H.; Shen, F. C.; Liu, J.; Lan, Y. Q. Rational Design of MOF/COF Hybrid Materials for Photocatalytic H<sub>2</sub> Evolution in the Presence of Sacrificial Electron Donors. *Angew. Chem. Int. Ed.* **2018**, *57*, 12106-12110.
- [13] Kampouri, S.; Nguyen, T. N.; Ireland, C. P.; Valizadeh, B.; Ebrahim, F. M.; Capano, G.; Ongari, D.; Mace, A.; Guijarro, N.; Sivula, K. Photocatalytic Hydrogen Generation From a Visible-Light Responsive Metal–Organic Framework System: the Impact of Nickel Phosphide Nanoparticles. *J. Mater. Chem. A.* **2018**, *6*, 2476-2481.